Heliyon

ELSEVIER

Received:
3 December 2018
Revised:
10 February 2019
Accepted:
22 February 2019

Cite as: G. Nagaraju, Mahesh Garvandha. Magnetohydrodynamic viscous fluid flow and heat transfer in a circular pipe under an externally applied constant suction. Heliyon 5 (2019) e01281. doi: 10.1016/j.heliyon.2019.e01281

Magnetohydrodynamic viscous fluid flow and heat transfer in a circular pipe under an externally applied constant suction

G. Nagaraju [a,*], **Mahesh Garvandha** [b]

[a] *Center for Research and Strategic Studies, Lebanese French University, Kurdistan Region, Erbil, Iraq*

[b] *Department of Mathematics, GITAM Deemed to be University, Hyderabad Campus, Rudraram, India*

[*] Corresponding author.

E-mail address: naganitw@gmail.com (G. Nagaraju).

Abstract

An analytical investigation of two-dimensional heat transfer behavior of an axisymmetric incompressible dissipative viscous fluid flow in a circular pipe is considered. The flow is subjected to an externally applied uniform suction over the pipe wall in the transverse direction and a constant magnetic field opposite to the wall. The reduced Navier-Stokes equations in the cylindrical system are applied for the velocity and temperature fields. Constant wall temperature is considered as the thermal boundary condition. The velocity components are expressed into stream function and its solution is acquired by the Homotopy analysis method (HAM). The effects of magnetic body force parameter(M), suction Reynolds number (Re), Prandtl number (Pr)and Eckert number (Ec) on velocity and temperature are examined and are presented in a graphical frame. Streamlines, isotherms and pressure contours are likewise pictured. It is observed that with increasing suction Reynold number decelerates axial flow, whereas it enhances the radial flow. The temperature distribution increases with an increase in Prandtl number, whereas it decreases with an increase in Eckert number (viscous dissipation effect).

Keywords: Applied mathematics, Electromagnetism, Mechanics, Thermodynamics

https://doi.org/10.1016/j.heliyon.2019.e01281

1. Introduction

Viscous flows in channels and pipes possess large amounts of mechanical applications which may incorporate cooling frameworks, petrochemical transport (oil and petroleum gas) and biotechnology. Regularly such flows are going with heat transfer and a representative example is the removal of thermal energy from hydronic space heating framework [1] by means of circling water in the heater, after which it is transported to the individual areas through pipes. Different frameworks utilizing heat transfer in viscous pipe flow are space thermal control [2], solar collectors [3] and heat exchangers [4].

In ongoing decades, engineers have additionally explored the change of viscous flows by means of porosity of the pipe or channel. Injection or evacuation of fluid by means of pores is a powerful instrument for flow control [5]. This innovation finds vital potential in biomedical sciences (e.g. counterfeit dialysis, blood flows) and in other topics, for example, rocket transpiration cooling and food preservation. Scientific demonstrating of flows in channels/pipes with wall mass flux has, in this manner, invigorated some enthusiasm for the examination network. Berman [6] was the first to examine the steady Newtonian flow in a permeable (porous) straight channel with uniform suction/injection impacts. Later Bansal [7] stretched out this work to a steady viscous flow through a porous circular pipe with the suction and axial pressure gradient. He found that the velocity accomplishes the greatest incentive along the axis of the pipe. An analytical solution for the laminar flow through circular pipes with steady suction/injection at the wall was further discussed by Terril [8, 9]. Tsangaris and Kondaxakis [10] examined unsteady viscous laminar flow in a straight pipe. They got an exact solution for time-changing infusion/suction at the permeable wall. Cox and Hill [11] have inspected the Newtonian fluid through carbon nanotubes with a Navier slip at the boundary. Ramana Murthy et. al [12]. investigated micropolar flow generated by a porous cylinder showing rotatory motions. They found that drag diminishes numerically when the suction parameter increments. Srinivas and Ramana Murthy [13] have examined wall suction effects in immiscible couple stress flow between two homogeneous permeable walls. They recognized that fluid velocity increments with Darcy number.

Magnetohydrodynamic (MHD) is additionally a functioning zone of present day engineering applications and includes the interaction between the applied magnetic fields and electrically conducting fluids. MHD pipe flows emerge in ionized accelators, MHD flow control in atomic reactors, MHD bypass energy generators, fluid metal manufacture forms, bubble levitation and so on [14]. MHD flows including suction/injection wall impacts have accumulated significant consideration. Terrill and Shrestha [15] presented an analytical study of laminar flow between two parallel porous plates with a connected magnetic field. They had demonstrated that the surface friction increments with the rise in magnetic number. Attia [16] examined the

https://doi.org/10.1016/j.heliyon.2019.e01281

unsteady flow through a circular pipe with axial pressure gradient applied for two-stage MHD non-Newtonian fluids. He found that with the stronger magnetic field, the velocity and temperature components for the two phases decrease. Attia and Ahmed [17] studied the unsteady flow through magnetized viscoplastic (Bingham) fluid in a circular pipe. They identified that skin friction enhances with particle-phase viscosity. El-Shahed [18] investigated the impacts of a transverse magnetic field and porous medium in second-grade fluid flow through a circular pipe. He obtained velocity solutions in terms of Fox's H-function. Ramana Murthy and Bahali [19]have examined the impacts of periodic suction/injection through magneto-micropolar flow in a permeable circular pipe. They identified that wall shear stress rises with the magnetic parameter. Ramana Murthy et al. [20] studied the effects of wall suction/blowing in hydromagnetic micropolar fluid through a rectangular channel. They found that the magnetic field reduces the flow rate sizes extensively. Mabood et al. [21]studied the impacts of MHD and radiation in chemically reactive nanofluid through a stretching surface. Mabood et al [22] investigated double-diffusive impacts in MHD, non-Darcian stretching sheet flow. Shateyi and Mabood [23] inspected mixed convection and stagnation point flow with radiation and viscous heating through the non-linear MHD stretching surface.

The above examinations overlooked viscous heating impacts which can apply a significant effect in numerous applications. It is realized that viscous dissipation adjusts the temperature distributions and acts as an energy source. This thusly particularly impacts heat transfer rates. The effect of viscous heating is firmly needy additionally on whether the pipe is being heated or cooled i.e. thermal boundary conditions at the pipe surface apply a important work in how much viscous heating changes the distribution of heat in viscous flows [24], In addition, viscous heating has been shown to play an enhanced role in fluids with low thermal conductivity and high viscosity. An essential investigation was conveyed by Gebhart [25] with regards to boundary layer flows. Historically, Brinkman started viscous heating [26] studies. Ou and Cheng [27] considered the impact of viscous dissipation on heat transfer at the inlet of a pipe with steady heat flux. Béget al. [28] obtained numerical solutions for the nonlinear flow and heat transfer of MHD Hartmann−Couette in a Darcian channel with porous medium and Ohmic dissipation. Other interesting and recent research into the thermo-fluid dynamics of pipes has been reported in [29, 30, 31, 32, 33, 34, 35, 36, 37].

To date, very few authors [27, 28, 29, 30, 31] have studied heat transfer in two-dimensional hydromagnetic convection flow in porous circular pipes/channels. Again, their results are not analytical and are obtained through FLUENT software or numerical methods. Therefore, in this case, analytical results are necessary and we aim to examine the analytical solution for the two-dimensional heat transfer effects in a circular pipe under externally applied uniform suction and magnetic field on the surface of the circular pipe. The transformed, non-dimensional boundary value problem is solved by the powerful Homotopy Analysis Method (HAM)

https://doi.org/10.1016/j.heliyon.2019.e01281

[38], which offers excellent flexibility and convergence features for non-linear ODE resolution. The method was successfully applied to a number of interesting problems [39, 40, 41, 42, 43, 44]. The present study relates to MHD energy systems.

2. Model

Consider an endlessly long cylinder of radius *a,* in which an electrically conducting viscous fluid is streaming, is appearing in Fig. 1. The thickness of the pipe is ignored and the mechanism of heat transfer is investigated through uniform wall temperature on the surface of the pipe. Since the pipe has an infinite length, the flow is developed completely. The flow is subjected to a uniform external suction in the normal direction through the wall. There is a uniform magnetic field of solidarity B_0 in the transverse direction (in contrast to the pipe wall) and no electric field outside is connected. The number of Magnetic Reynolds is sufficiently small to discredit incited magnetic field impacts. When modified for the magnetic body force effect, the primitive equations for the steady, axi-symmetric, incompressible Newtonian fluid flow (Bird et al. [45]) are shown to take the form:

$$\frac{\partial U}{\partial R}+\frac{U}{R}+\frac{\partial W}{\partial Z}=0 \tag{1}$$

$$\rho\left(U\frac{\partial U}{\partial R}+W\frac{\partial U}{\partial Z}\right)=-\frac{\partial P}{\partial R}+\mu\frac{\partial}{\partial Z}\left(\frac{\partial U}{\partial Z}-\frac{\partial W}{\partial R}\right)-\sigma B_0^2 U \tag{2}$$

$$\rho\left(U\frac{\partial W}{\partial R}+W\frac{\partial W}{\partial Z}\right)=-\frac{\partial P}{\partial Z}-\frac{\mu}{R}\frac{\partial}{\partial R}\left(R\left(\frac{\partial U}{\partial Z}-\frac{\partial W}{\partial R}\right)\right)-\sigma B_0^2 W \tag{3}$$

$$\rho c_p\left(U\frac{\partial T}{\partial R}+W\frac{\partial T}{\partial Z}\right)=k_T\left(\frac{\partial^2 T}{\partial R^2}+\frac{1}{R}\frac{\partial T}{\partial R}+\frac{\partial^2 T}{\partial Z^2}\right)+\mu\left\{2\left[\left(\frac{\partial U}{\partial R}\right)^2+\left(\frac{\partial W}{\partial Z}\right)^2+\left(\frac{U}{R}\right)^2\right]+\left(\frac{\partial U}{\partial Z}+\frac{\partial W}{\partial R}\right)^2\right\} \tag{4}$$

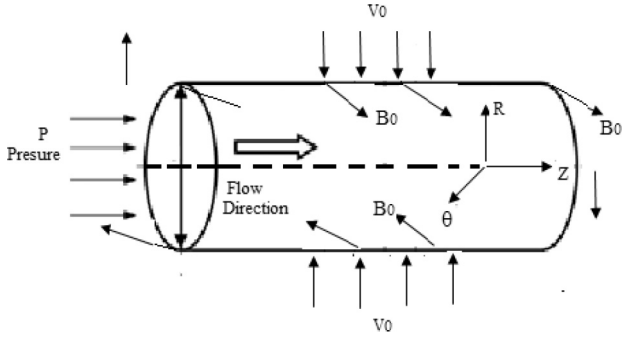

Fig. 1. Schematic diagram.

https://doi.org/10.1016/j.heliyon.2019.e01281

where (U, W) are the velocity parts in (R,Z) bearings separately, P is pressure, ?? is the density of the fluid, ?? is viscosity, σ is electrical conductivity, c_p is the specific heat at consistent pressure, T is the temperature of the liquid and k_T is thermal conductivity. It is relevant to present the accompanying non-dimensional parameters, where capitalized letters signify physical (dimensional) amounts and lowercase letters speak to the relating non-dimensional amounts:

$$u = \frac{U}{v_0},\ w = \frac{W}{v_0},\ r = \frac{R}{a},\ p = \frac{P}{\rho v_0^2},\ z = \frac{Z}{a},\ \theta = \frac{T}{T_1} \tag{5}$$

Here T_1 is constant temperature at the surface.

Executing condition (5) into conditions (1)−(4), following dimensionless arrangement of coupled differential equations, develops:

$$\frac{\partial u}{\partial r} + \frac{u}{r} + \frac{\partial w}{\partial z} = 0 \tag{6}$$

$$Re\left(u\frac{\partial u}{\partial r} + w\frac{\partial u}{\partial z}\right) = -Re\frac{\partial p}{\partial r} + \frac{\partial}{\partial z}\left(\frac{\partial u}{\partial z} - \frac{\partial w}{\partial r}\right) - M^2 u \tag{7}$$

$$Re\left(u\frac{\partial w}{\partial r} + w\frac{\partial w}{\partial z}\right) = -Re\frac{\partial p}{\partial z} - \frac{1}{r}\frac{\partial}{\partial r}\left(r\left(\frac{\partial u}{\partial z} - \frac{\partial w}{\partial r}\right)\right) - M^2 w \tag{8}$$

$$RePr\left(u\frac{\partial \theta}{\partial r} + w\frac{\partial \theta}{\partial z}\right) = Ec\varphi + \nabla^2\theta \tag{9}$$

Here the dissipation function φ is given by$\varphi = 2\left[\left(\frac{\partial u}{\partial r}\right)^2 + \left(\frac{\partial w}{\partial z}\right)^2 + \left(\frac{u}{r}\right)^2\right] + \left(\frac{\partial u}{\partial z} + \frac{\partial w}{\partial r}\right)^2$, the Laplacian operator defined as$\nabla^2 = \frac{\partial^2\theta}{\partial r^2} + \frac{1}{r}\frac{\partial \theta}{\partial r} + \frac{\partial^2\theta}{\partial z^2}$, Re $= \frac{\rho v_0 a}{\mu}$, $M^2 = \frac{\sigma B_0^2 a^2}{\mu}$, $Pr = \frac{\mu c_p}{k_T}$ and $Ec = \frac{\mu v_0^2}{k_T T_1}$ where Re is suction Reynolds number, M is the magnetic body force parameter (ratio of hydromagnetic and viscous body forces), Pr is Prandtl number, and Ec is the Eckert number (viscous heating parameter).

Since the flow is two dimensional, a stream function ψ may be defined to satisfy the mass conservation (continuity) Eq. (6):

$$u = -\frac{1}{r}\frac{\partial \psi}{\partial z},\ w = \frac{1}{r}\frac{\partial \psi}{\partial r} \tag{10}$$

Eliminating the pressure gradient termsfrom (7) and (8),yields:

https://doi.org/10.1016/j.heliyon.2019.e01281

$$Re\left(-\frac{2}{r^3}\frac{\partial\psi}{\partial z}E^2\psi+\frac{1}{r^2}\left(\frac{\partial\psi}{\partial z}\frac{\partial E^2\psi}{\partial r}-\frac{\partial\psi}{\partial r}\frac{\partial E^2\psi}{\partial z}\right)\right)=\frac{-1}{r}E^2\left(E^2\psi\right)+\frac{M^2}{r}E^2\psi \tag{11}$$

where $E^2=\frac{\partial^2}{\partial r^2}-\frac{1}{r}\frac{\partial}{\partial r}+\frac{\partial^2}{\partial z^2}$ is the stokes function operator

Following Terril and Shresta [15], ψ is assumed to take the following form

$$\psi=(N-z)f(r) \tag{12}$$

Where N= U_0/v_0, U_0 is the entrance velocity, v_0 is suction velocity (pipe surface lateral mass flux).

$$Re\left(\frac{3ff''}{r^2}-\frac{3ff'}{r^3}-\frac{ff'''}{r}+\frac{f'f''}{r}-\frac{f'^2}{r^2}\right)=-D^2\left(D^2-M^2\right)f \tag{13}$$

where $D^2=\frac{d^2}{dr^2}-\frac{1}{r}\frac{d}{dr}$ is a differential operator.

Eq. (13) is to be solved under the boundary conditions given by:

$$\left.\begin{array}{l}
\text{(i) On the z}-\text{axis } u=0.\ \text{i.e., at } r=0,\ u=0 \text{ this implies } \lim_{r\to 0}\frac{1}{r}f(r)=0,\\
\text{i.e., } f(0)=0.\\
\text{(ii) The flow is maximum along } r=0.\ \text{i.e., w is maximum on } r=0,\ \text{i.e}\frac{dw}{dr}=0,\\
\text{i.e., } D^2f=0 \text{ at } r=0\\
\text{(iii) A suction velocity } v_0 \text{ is imposed on the surface of the pipe. In dimensional less form,}\\
\text{on } r=1,\ u=v_0 \text{ suction velocity.}\\
\text{i.e., } f(1)=1.\\
\text{(iv) } w=0 \text{ at } r=1 \text{(No slip condition): i.e, } f'(1)=0\\
\text{(v) } T=T_1 \text{ at r} =1,\ \text{i.e., } \theta(1)=1 \text{ (On the surface, temperature is constant)}\\
\text{(vi) } \frac{\partial T}{\partial r}=0 \text{ at r} =0 \text{ i.e., } \theta'(0)=0 \text{(On the axis of pipe)}
\end{array}\right\} \tag{14}$$

3. Methodology

The Eqs. (13) and (9) are fathomed utilizing HAM. This system was presented by Liao [38] during the 1990s. HAM depends on the homotopy of topology and is similarly adroit at explaining nonlinear ordinary and partial differential equation systems and has been utilized broadly in heat transfer, magnetic fluid dynamics, non-Newtonian and Newtonian flows. Late precedents incorporate [46, 47].

To create systematic arrangements by HAM, the differential Eqs. (13) and (9) are put in the accompanying homotopy shape, which is known as the zeroth request distortion equation, as

https://doi.org/10.1016/j.heliyon.2019.e01281

$$(1-\lambda)L_1[fh(r,\lambda)-f_0(r)]=\lambda h_1 HN_1(fh) \tag{15}$$

Where

$$N_1[fh(r,\lambda)]=-D^2\left(D^2-M^2\right)fh$$

$$-\frac{Re}{r^3}\left(3rfh\frac{\partial^2 fh}{\partial r^2}-3fh\frac{\partial fh}{\partial r}-r^2 fh\frac{\partial^3 fh}{\partial r^3}+r^2\frac{\partial fh}{\partial r}\frac{\partial^2 fh}{\partial r^2}-r\left(\frac{\partial fh}{\partial r}\right)^2\right). \tag{16}$$

$$(1-\lambda)L_2[\theta h(r,z,\lambda)-\theta_0(r)]=\lambda h_2 HN_2(\theta h,fh) \tag{17}$$

where

$$\begin{aligned}N_2(\theta h(r,z,\lambda))=RePr\Bigg(&\frac{fh}{r}\left((N-z)^2\frac{\partial\theta_1}{\partial r}+\frac{\partial\theta_2}{\partial r}\right)-2\frac{(N-z)^2}{r}\theta_1\frac{\partial fh}{\partial r}\Bigg)\\&-Ec\Bigg\{2\left[\left(\frac{1}{r}\frac{\partial fh}{\partial r}-\frac{fh}{r^2}\right)^2+\left(\frac{1}{r}\frac{\partial fh}{\partial r}\right)^2+\left(\frac{f(r,\lambda)}{r^2}\right)^2\right]\\&+(N-z)^2\left(\frac{1}{r}\frac{\partial^2 fh}{\partial r^2}-\frac{\partial fh}{r^2\partial r}\right)^2\Bigg\}-\Bigg((N-z)^2\left(\frac{\partial^2\theta_1}{\partial r^2}+\frac{1}{r}\frac{\partial\theta_1}{\partial r}\right)\\&+\left(\frac{\partial^2\theta_2}{\partial r^2}+\frac{1}{r}\frac{\partial\theta_2}{\partial r}+2\theta_1\right)\Bigg)\end{aligned} \tag{18}$$

With

$$\theta(r,z,\lambda)=(N-z)^2\theta_1(r,\lambda)+\theta_2(r,\lambda). \tag{19}$$

In the above λ is the homotopy parameter, h_1, $h_2$are convergence control parameters, $fh$and θh are the homotopy functions which are taken as f_0 and θ_0 when $\lambda = 0$ and approaches f and θ as $\lambda \to 1$. The differential operators$L_1$and L_2 are linear and can be chosen at our convenience and $N_1(fh)$ =0 and $N_2(\theta h)$=0 are the original nonlinear problems for f and θ which can be obtained as $\lambda \to 1$. The initial functions f_0 and θ_0 when $\lambda = 0$ satisfy $L_1(f_0)$=0 and $L_2(\theta_0)$=0 and the boundary conditions of the problem. Here, the auxiliary function H is taken as 1.

For our problem, the initial approximations $f_0$and $\theta_0$and auxiliary linear operators $L_1$and $L_2$are taken as follows:

$$f_0=r^2\left(2-r^2\right) \text{ and } \theta_0(r)=1 \tag{20}$$

https://doi.org/10.1016/j.heliyon.2019.e01281

$$L_1[f] = D^4 f \text{ and } L_2[\theta] = \nabla^2 \theta \tag{21}$$

With

$$L_1\left[c_1 r^4 + c_2 r^2 (2\log r - 1) + c_3 r^2 + c_4\right] = 0, \tag{22}$$

Table 1. Correlation of the consequences of radial velocity by HAM and that arrangement given in [31].

Distance r	Radial velocity(*f*), Numerical solution by Ben-Mansour and Sahin [31]	Radial velocity(*f*), Present solution by HAM (15th order approximation)
0	0.0000046	0
0.2	0.057945	0.0581946
0.4	0.196226	0.206445
0.6	0.498711	0.498719
0.8	0.811455	0.811468
1	1.002766	1

To approve our results, we have contrasted them and the past non-magnetic (M = 0) arrangements of Ben-Mansour and Sahin [31] with the accompanying recommended information: Re = 5, N = 2, z = 0.5 and these are archived in Table 1. The relationship is close and thusly trust in the present arrangements is reasonably high. The table likewise unmistakably exhibits the noteworthy improvement in radial velocity with expanding distance.

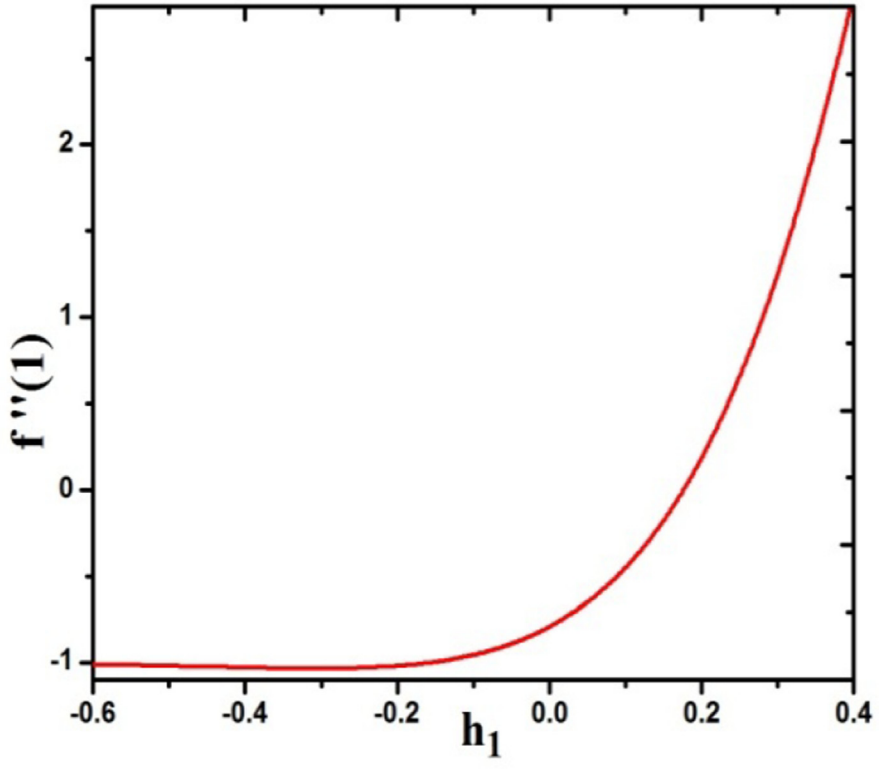

Fig. 2. h curve for f(r).

https://doi.org/10.1016/j.heliyon.2019.e01281

$$L_2\left[(N-z)^2(c_5+c_6 log r)+c_7 r^2+c_8 r^2(log r-1)\right]=0 \tag{23}$$

The homotopy functions fh for $f$and θh for θ are assumed as follows;

$$fh = f_0 + \lambda f_1 + \ldots + \lambda^n f_n + \ldots \tag{24}$$

$$\theta h = \theta_0 + \lambda \theta_1 + \ldots + \lambda^n \theta_n + \ldots \tag{25}$$

These functions fh in (24) and θh in (25) are substituted in (15) and (17) and coefficient of $\lambda^n$to get the ***n^th order deformation equations*** viz.,

$$L_1[f_n(r) - \Upsilon_n f_{n-1}(r)] = h_1 R_{1,n}(r) \tag{26}$$

$$L_2[\theta_n(r) - \Upsilon_n \theta_{n-1}(r)] = h_2 R_{2,n}(r) \tag{27}$$

Where

$$R_{1,n}(r) = -D^2\left(D^2 - M^2\right) f_{n-1}$$

$$-\frac{Re}{r^3}\sum_{i=0}^{n-1}\left(3rf_i f''_{n-1-i} - 3f_i f'_{n-1-i} - r^2 f_i f'''_{n-1-i} + r^2 f'_i f''_{n-1-i} - r f'_i f'_{n-1-i}\right) \tag{28}$$

and

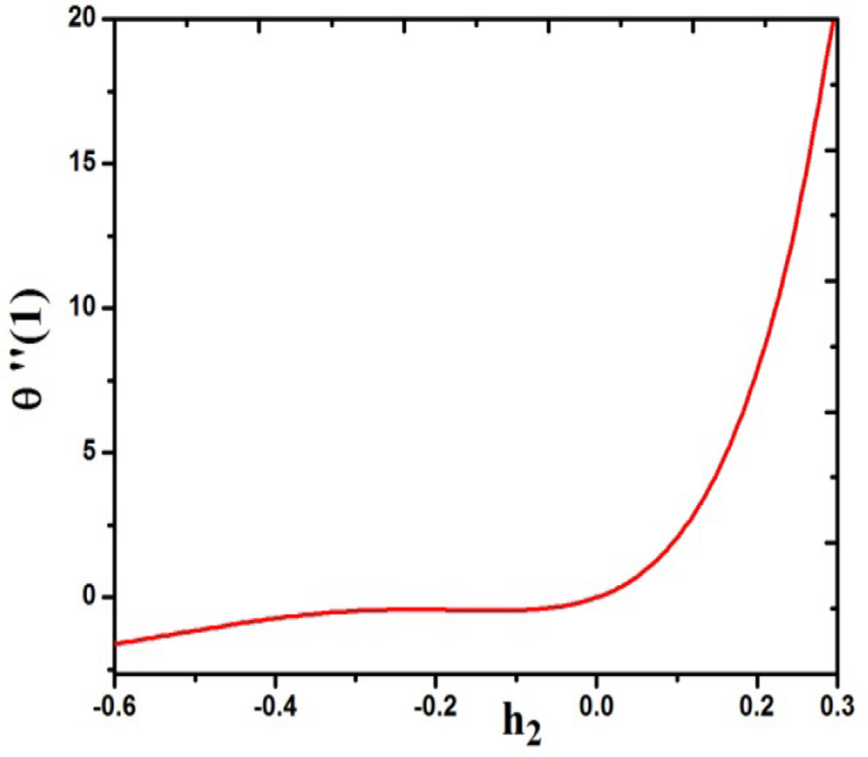

Fig. 3. h curve for θ(r).

https://doi.org/10.1016/j.heliyon.2019.e01281

$$R_{2,n}(r) = \nabla^2\theta_{n-1} - RePr\sum_{i=0}^{n-1}\left((N-z)^2\left(\frac{f_i}{r}\theta'_{1,n-1-i} - \frac{2}{r}\theta_{1,n-1-i}f'_i\right) + \frac{f_i}{r}\theta'_{2,n-1-i}\right)$$
$$+ Ec\sum_{i=0}^{n-1}\left(2\left(\frac{f_i}{r}\right)'\left(\frac{f_{n-1-i}}{r}\right)' + \frac{2}{r^2}f'_i f'_{n-1-i} + \frac{2}{r^4}f_i f_{n-1-i}\right.$$
$$\left. + (N-z)^2\left(\frac{f'_i}{r}\right)'\left(\frac{f'_{n-1-i}}{r}\right)'\right) \tag{29}$$

and $\Upsilon_n = \begin{cases} 1, & n \neq 1 \\ 0, & n = 1 \end{cases}$.

The corresponding boundary conditions are

$$f_n(0) = D^2 f_n(0) = f_n(1) = f'_n(1) = \theta_n(1) = \theta\prime_n(0) = 0 \tag{30}$$

To solve Eqs. (26) and (27) with the conditions Eq. (30), we use the symbolic computation software *Mathematica*. We select $h_1$and h_2, properly in such a way

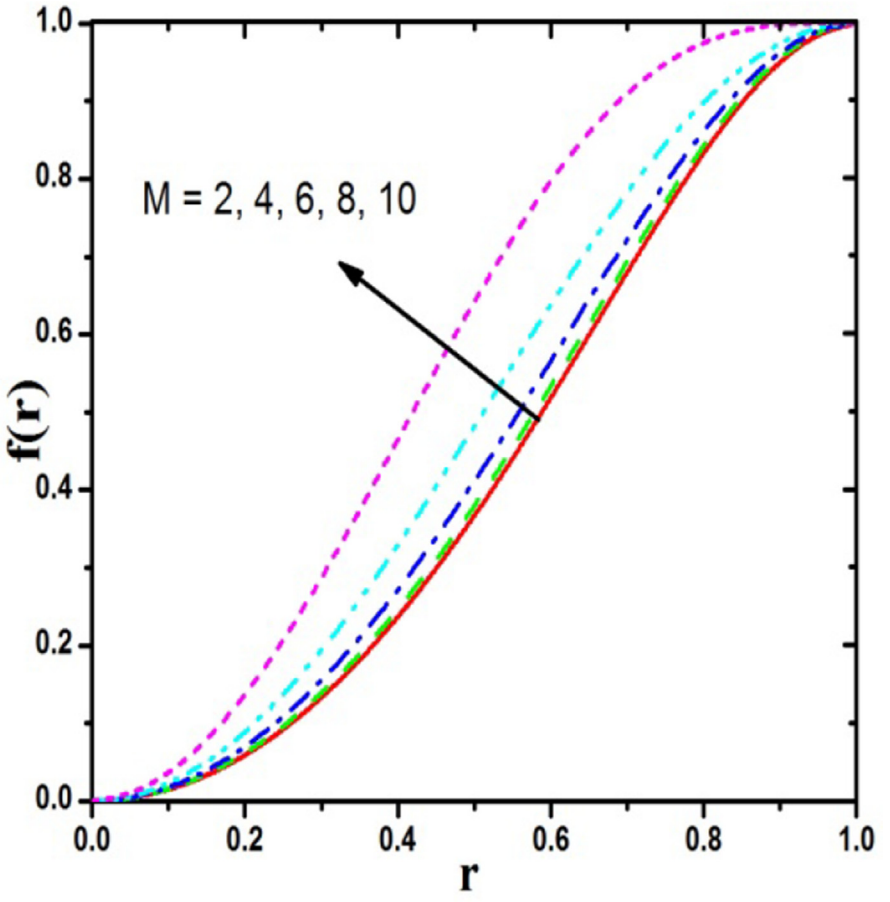

Fig. 4. Response of M on Radial velocity f.

https://doi.org/10.1016/j.heliyon.2019.e01281

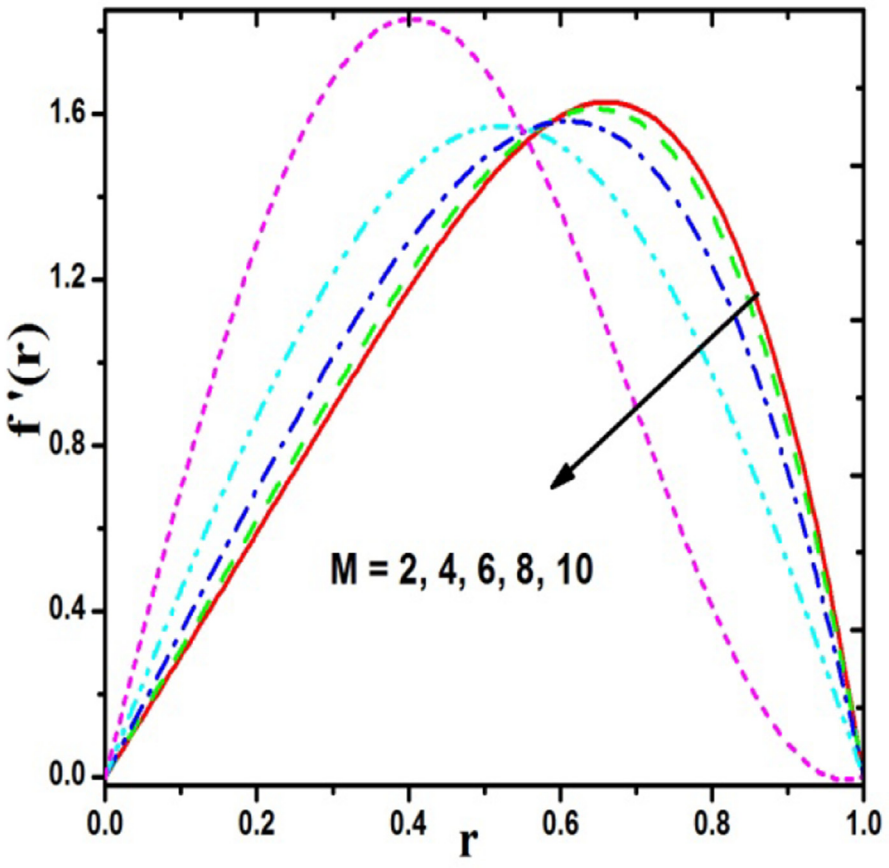

Fig. 5. Response of M on axial velocity f'.

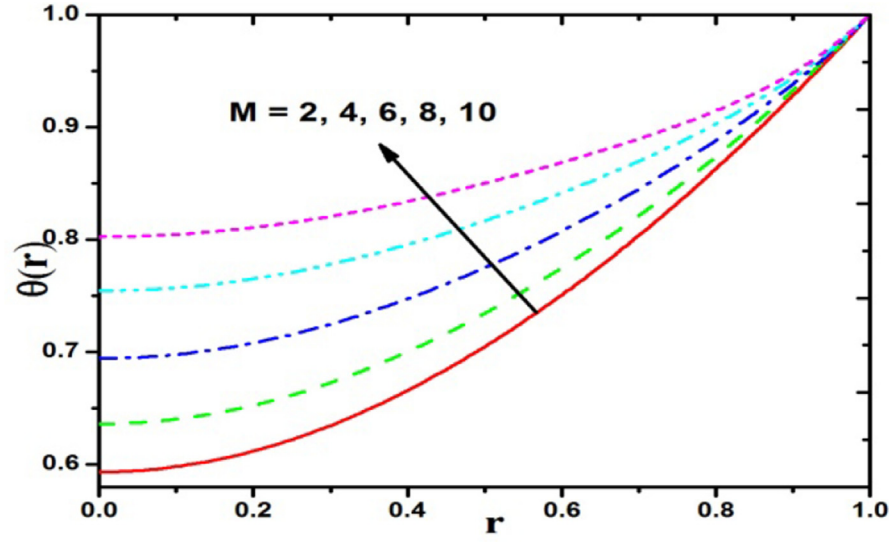

Fig. 6. Response of M on temperature θ.

https://doi.org/10.1016/j.heliyon.2019.e01281

that these series are convergent at $\lambda = 1$, therefore we have the expressions as follows:

$$f(r) = f_0(r) + \sum_{n=1}^{\infty} f_n(r) \tag{31}$$

$$\theta(r) = \theta_0(r) + \sum_{n=1}^{\infty} \theta_n(r) \tag{32}$$

The dimensionless form for pressure(p), from Eqs. (7) and (8), is given by

$$Re\frac{\partial p}{\partial r} = Re\left(\frac{f^2}{r^3} - \frac{ff'}{r^2}\right) - \frac{(D^2 - M^2)f}{r}$$

$$Re\frac{\partial p}{\partial z} = -\frac{N-z}{r}\left\{\frac{d}{dr}(D^2 - M^2)f + Re\left(\frac{ff''}{r} - \frac{ff'}{r^2} - \frac{(f')^2}{r}\right)\right\} \tag{33}$$

Assume $p = p_1(r) + (N-z)^2 p_2(r)$, inspection gives :

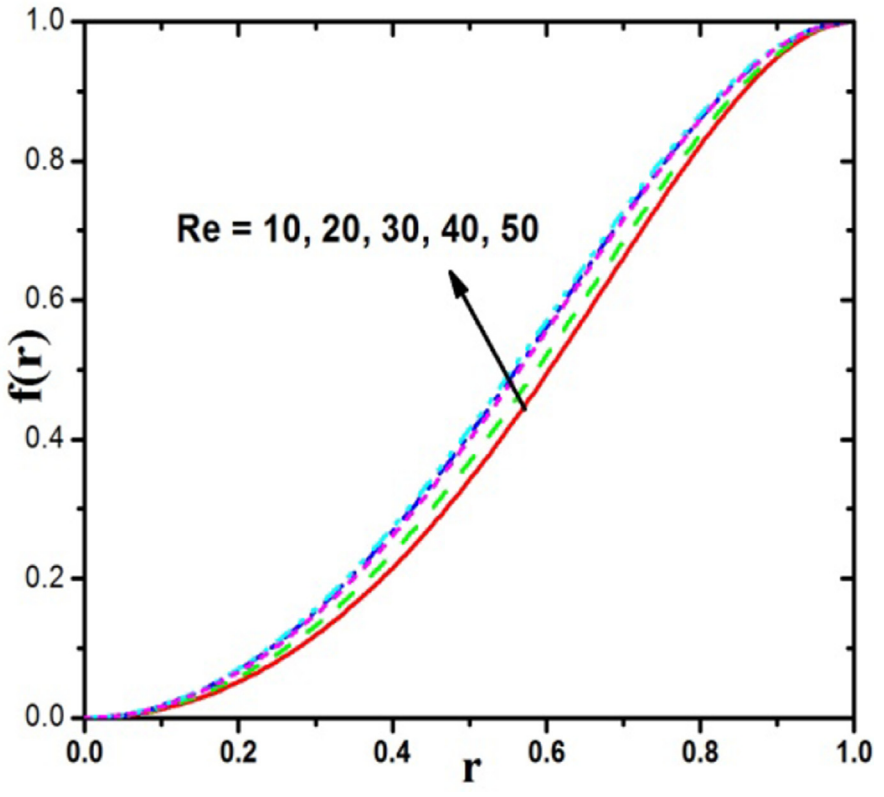

Fig. 7. Reynolds number effect on f.

https://doi.org/10.1016/j.heliyon.2019.e01281

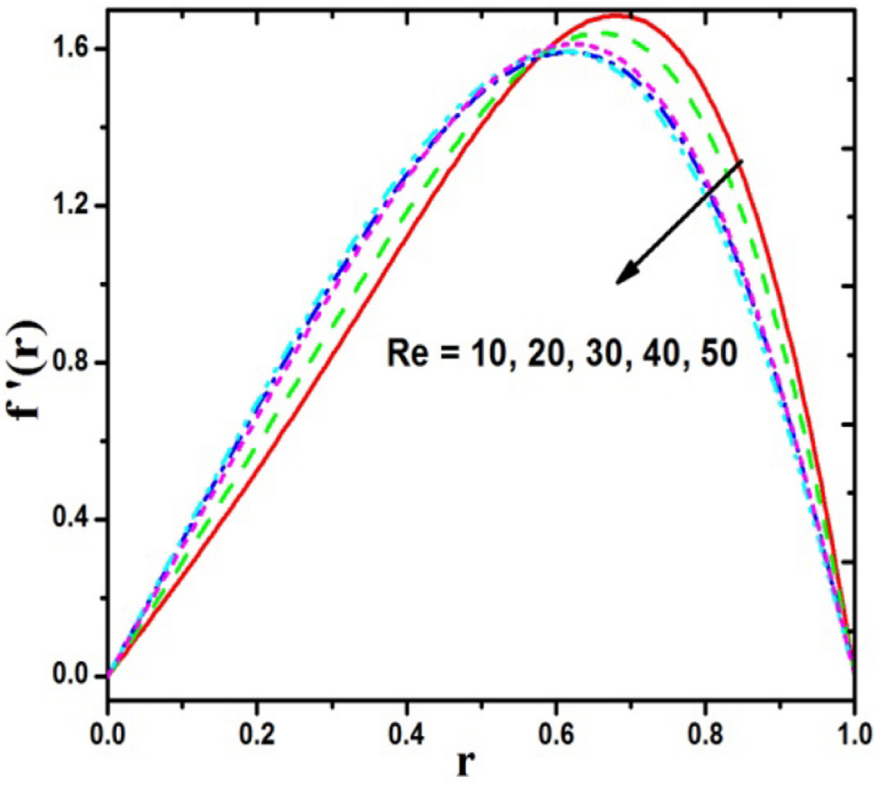

Fig. 8. Reynolds number effect on *f*′.

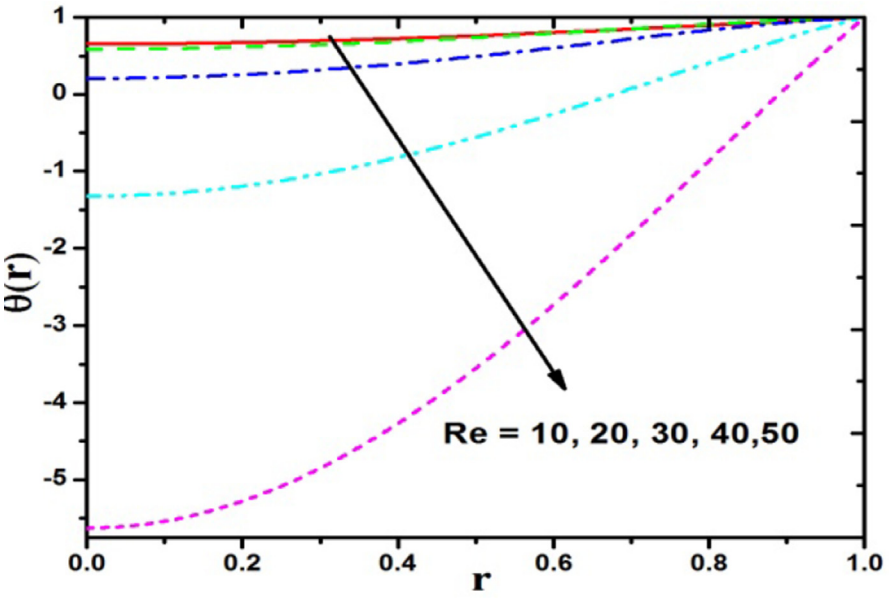

Fig. 9. Reynolds number effect on θ.

https://doi.org/10.1016/j.heliyon.2019.e01281

$$p_2 = \text{constant and } p_1 = \int \left\{ \frac{-1}{r}\left(\frac{ff'}{r} - \frac{f^2}{r^2}\right) - \frac{1}{rRe}(D^2 - M^2)f \right\} dr \tag{34}$$

The shear stress T_{rz} at the pipe wall is given by

$$T_{rz} = \mu\left(\frac{\partial W}{\partial R} + \frac{\partial U}{\partial R}\right) = \frac{\mu}{av_0}\frac{(N-z)}{r}D^2 f \tag{35}$$

Hence the coefficient of skin friction $C_f = \frac{2T_{rz}}{\rho v_0^2}$ on r = 1is given by

$$C_f = \frac{2(N-z)}{Re}D^2 f \text{ at r} = 1 \tag{36}$$

The rate of heat transfer (heat flux) is given by $q_w = -k_T \left.\frac{\partial T}{\partial R}\right|_{R=a}$ (37)

The dimensionless heat flux may be expressed by $Nu = \frac{aq_w}{k_T T_1}$ (38)

where Nu is the Nusselt number.

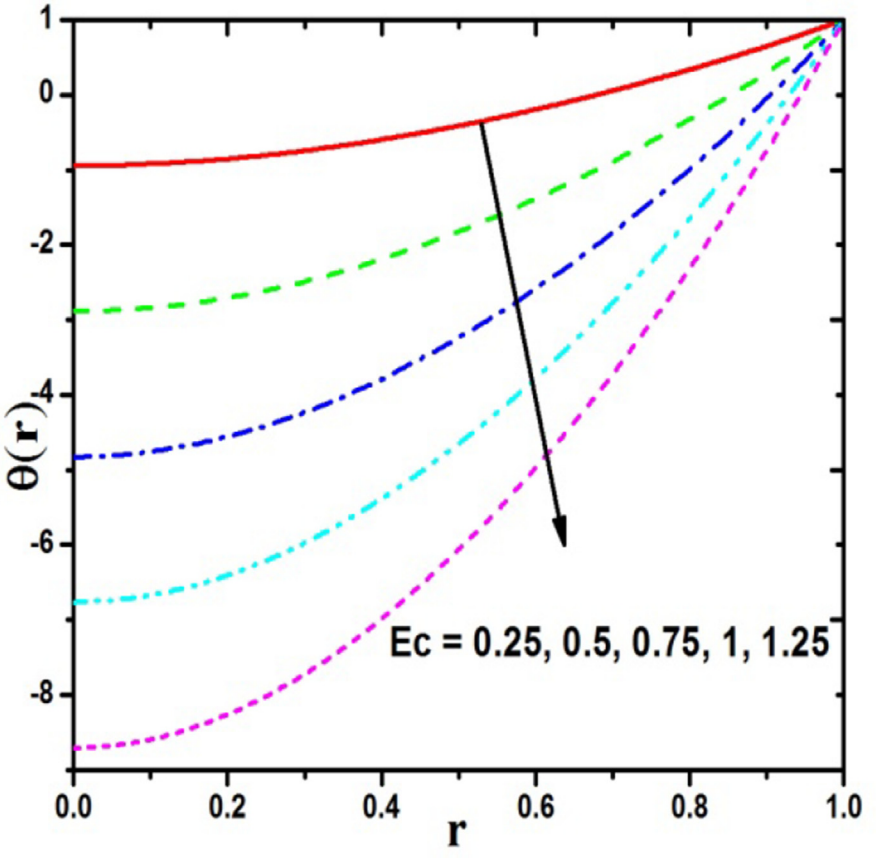

Fig. 10. Eckert number effect on θ.

https://doi.org/10.1016/j.heliyon.2019.e01281

From (37) and (38), the Nusselt number takes the form $Nu = -\left.\frac{\partial\theta}{\partial r}\right|_{r=1}$ (39)

4. Results & discussions

A parametric investigation of the impact of the key thermophysical parameters on velocity and temperature capacities is led. To guarantee combination is accomplished we initially expand on this viewpoint. Calculations were done by setting up the parameters M = 5, Re = 10, Pr = 0.7 and Ec = 0.45 to examine the impacts of the rising parameters.

The velocity and temperature articulations contain the auxiliary parameters h_1 and h_2. As pointed out by Liao [38], the assembly and the rate of approximation for the HAM arrangement unequivocally rely upon the estimations of auxiliary parameter h. For this reason, h-curves are plotted for deciding the scopes of h_1 and h_2. The estimations of and from the h-curves are envisioned in Figs. 2 and 3 for the 10th-

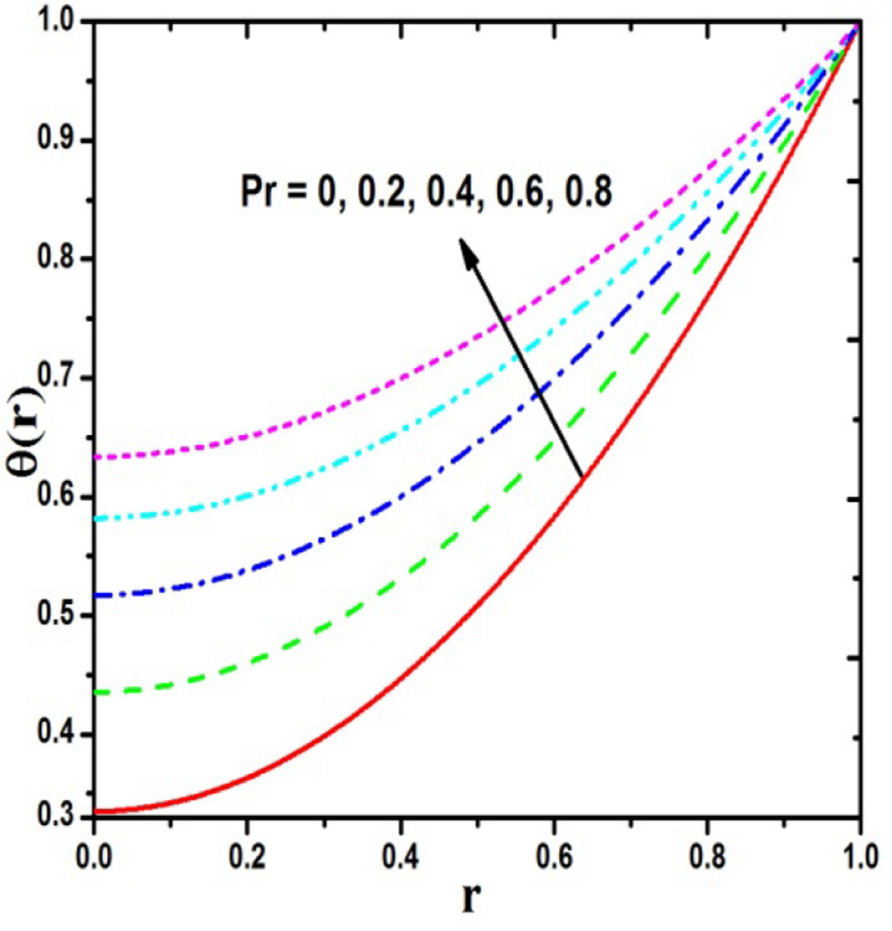

Fig. 11. Prandtl number effect on θ.

https://doi.org/10.1016/j.heliyon.2019.e01281

order of approximation. It is clear that the range for the allowable estimations of h1 from Fig. 2 is $-0.6 < h_1 < -0.2$and from Fig. 3, the range for is $-0.6 < h_2 < 0$. We have chosen $h_1 = -0.12$and $h_2 = -0.1$. Superb convergence is accomplished for the 10th order approximation which is embraced in every single consequent calculation and figures. Here highly precise arrangements are therefore achieved with $h_1 = -0.25$, $h_2 = -0.1$.

Figs. 4, 5, 6 demonstrates the impact of the magnetic parameter on radial velocity f, axial velocity *f'* and temperature. It tends to be seen from the Figs. 4 and 6 that the radial velocity and temperature profiles are both upgraded with an expansion in the parameter M, while the axial velocity changes are at first expanded for lower radial organize values and therefore decreased for higher radial facilitate values. The radial increasing speed and axial deceleration are because of the Lorentzian magnetic body powers, emerging in the changed energy preservation Eq. (13). These powers reliably quicken the radial flow(f) across the pipe cross-section, while their impact on the axial stream is subject to the area i.e. radial arrange. From Fig. 6, it is obvious that as magnetic parameter builds, the temperature likewise increments. The valuable work consumed in hauling the liquid against the activity of a magnetic field the axial way is disseminated as warm vitality. This warms the liquid and

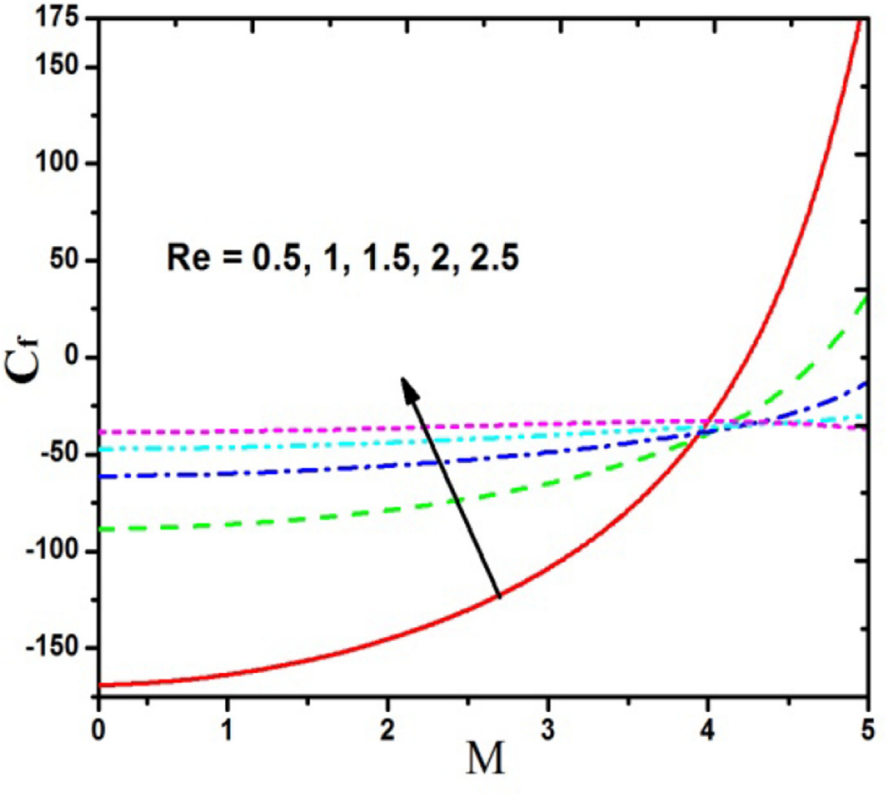

Fig. 12. Skin friction effect *on Re*.

https://doi.org/10.1016/j.heliyon.2019.e01281

accordingly raises temperatures in the gooey liquid. The temperature profiles all join asymptotically to a most extreme at the pipe surface (divider). These patterns are steady with numerous different examinations e.g. Gardner [48] and Cunha and Sobral [49].

From Fig. 7, obviously as Re expands, the radial velocity f likewise increments. From Fig. 8, we see that as Re expands, the most extreme estimations of *f*' (axial velocity) are lessened. This is perception is inverse to the impact of a magnetic parameter which improves the most extreme estimations of *f*'. This might be because of the way that more noteworthy Reynolds number suggests a more noteworthy inertial power in the routine in respect to thick power and this serves to quicken the radial stream. Reynolds number can't prompt a power the opposite way as on account of magnetic parameter M. It is additionally obvious from Fig. 9 that as Reynolds number increments, temperature(θ) profiles diminish definitely close to the pivot of the chamber. This shows as *Re* builds, warm dissemination in the laminar routine is repressed.

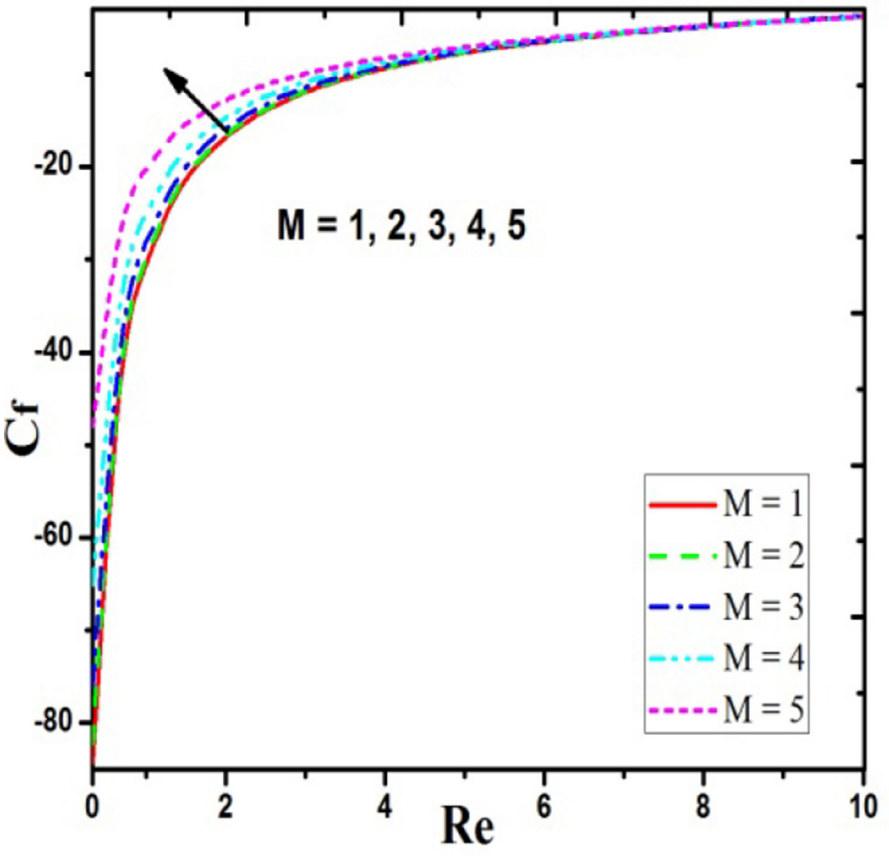

Fig. 13. Skin friction effect on *M*.

https://doi.org/10.1016/j.heliyon.2019.e01281

From Figs. 10 and 11, we see that as Eckert number (Ec) builds temperature close to the pipe hub diminishes and as Prandtl number (Pr) expands, temperature increments. The clashing conduct of Prandtl and Eckert numbers is outstanding in heat transfer.

In Fig. 12, it is discovered that Cf diminishes emphatically as suction Re increments, and accomplishes a steady an incentive after Re increments past 5. In Fig. 13 Cf diminishes altogether with more noteworthy magnetic parameter (M) until the point that Re increments past 5. In any case, for substantial qualities Re every one of the charts unite and consequent change in skin friction isn't found. The impact of magnetic power at lower Re esteems is plainly to restrain the flow i.e. prompt deceleration and decline skin friction.

In Fig. 14 obviously Nu sizes diminish Pr increments. A solid decrease in Nusselt number is additionally joined by more noteworthy Eckert number (Ec). Fig. 15 demonstrates that numerically diminishes up to a basic Prandtl number (Pr) and from that point increments essentially towards the surface of the pipe with expanding estimations of Re.

From Fig. 16, it is seen that the streamlines for $z \leq N$are non-neative and negative for $z > N$.Streamlines are numerically symmetric about $z = N$ line. From Fig. 17, it is seen that temperature is symmetric about $z = N$ line. The temperature is most

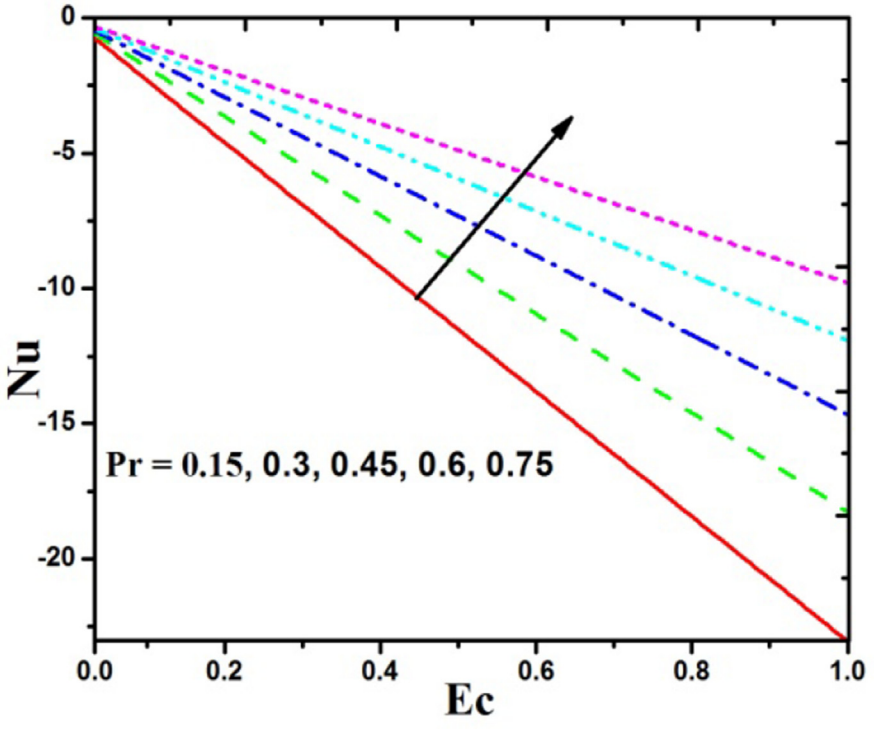

Fig. 14. Nusselt number effect on Pr.

https://doi.org/10.1016/j.heliyon.2019.e01281

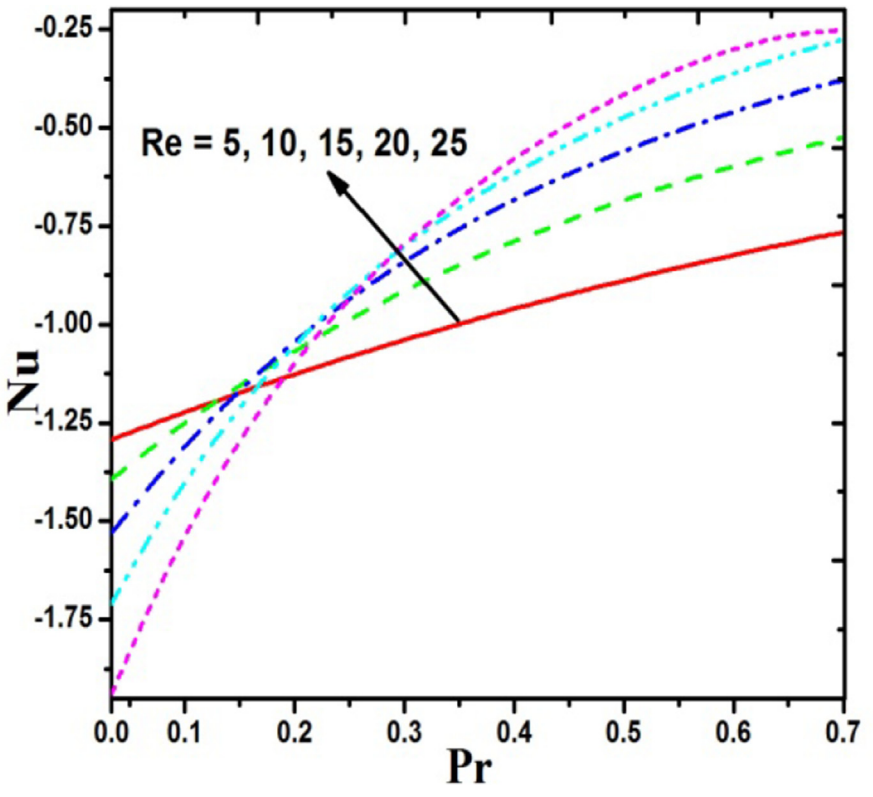

Fig. 15. Nusselt number effect on Re.

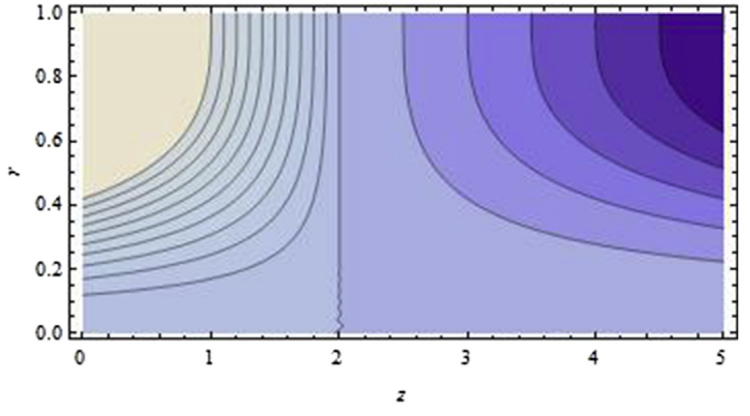

Fig. 16. Stream lines for velocity.

extreme close to pivot of the cylinder (since in that area progressive white shading is available). Most noteworthy temperature happens at $z = N$and this greatest esteem increments from r = 1 to r = 0. From Fig. 18, we can see that presure is symmetric about $z = N$and diminishes as $r \geq 0.5$and increments as $r < 0.5$. pressure is relatively consistent for $z < 1$ and $r < 0.5$ and again in the district $z > 3$, $r \leq 0.5$. Pressure changes significantly just in the area $1 < z < 3$.

https://doi.org/10.1016/j.heliyon.2019.e01281

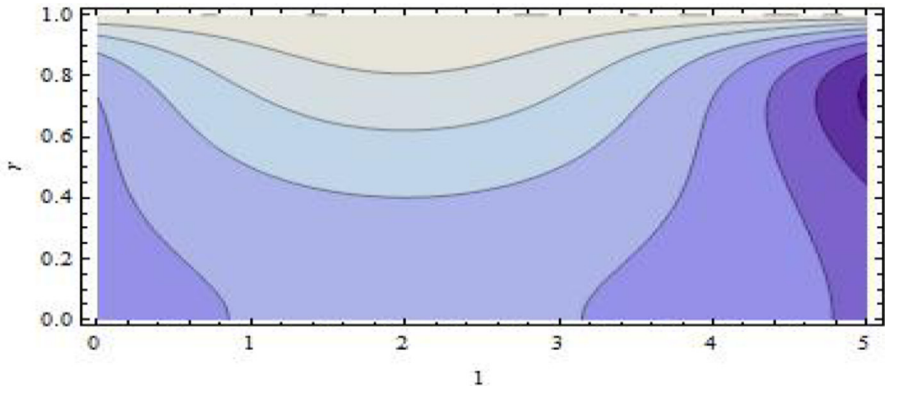

Fig. 17. Contour graphs for temparature.

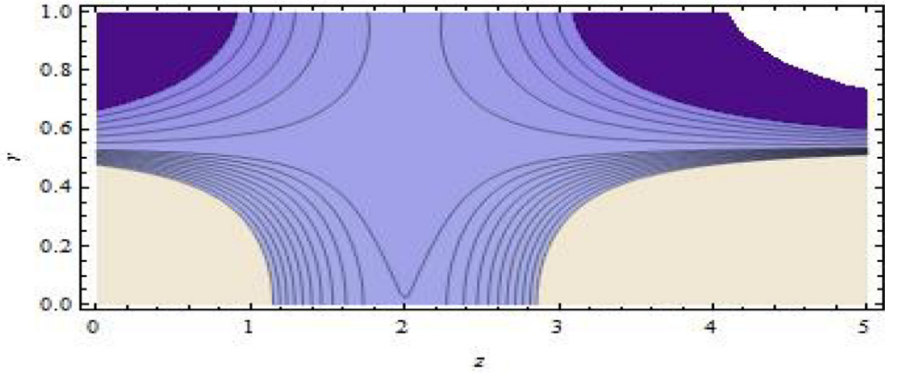

Fig. 18. Contour graphs for presure.

5. Conclusions

Analytical solutions for the thermal transfer of viscous magneto-hydrodynamic pipe flow using the homotopy analysis method (HAM) have been presented. Viscous heating, Mhd and suction/injection effects of the wall have been included. A HAM convergence study was also carried out to guarantee the robustness of the series solutions. The calculations showed that:

- ➢ Increasing magnetic body force parameter quickens the radial flow while it will in general decelerate axial flow.
- ➢ Increasing the magnetic parameter improves temperatures since it produces thermal energy dissemination attributable to the additional work required to drag the liquid against the magnetic field the pivotal way.
- ➢ Increasing suction Reynolds number decelerates the axial flow and upgrades the radial flow.
- ➢ With expanding Eckert number, the temperature along the outspread course is diminishing while with expanding Prandtl number it is raised.

https://doi.org/10.1016/j.heliyon.2019.e01281

➢ Skin friction is almost constant after a certain range of suction Reynolds number for all magnetic parameter values i.e. for low Reynolds numbers, the effect of magnetic parameter is significant.

Declarations

Author contribution statement

G. Nagaraju: Performed the experiments; Contributed reagents, materials, analysis tools or data; Wrote the paper.

Mahesh Garvandha: Conceived and designed the experiments; Analyzed and interpreted the data.

Funding statement

This research did not receive any specific grant from funding agencies in the public, commercial, or not-for-profit sectors.

Competing interest statement

The authors declare no conflict of interest.

Additional information

No additional information is available for this paper.

References

[1] K.N. Rhee, M.S. Yeo, K.W. Kim, Evaluation of the control performance of hydronic radiant heating systems based on the emulation using hardware-in-the-loop, Build. Environ. 46 (2011) 2012−2022.

[2] K.L. Walker, C. Tarau, W.G. Anderson, Grooved and self-venting arterial heat pipes for space fission power systems, Heat Pipe Science and Technology, Int. J. 5 (1-4) (2014) 507−514.

[3] H.M.S. Hussein, M.A. Mohamad, A.S. El-Asfouri, Optimization of a wickless heat pipe flat plate solar collector, Energy Convers. Manag. 40 (1999) 1949−1961.

[4] Leonard L. Vasilev, Heat pipes in modern heat exchangers, Appl. Therm. Eng. 25 (2005) 1−19.

[5] C.L. Tien, Fluid mechanics of heat pipes, Annu. Rev. Fluid Mech. 7 (1975) 167−185.

https://doi.org/10.1016/j.heliyon.2019.e01281

[6] A.S. Berman, Laminar flow in channels with porous walls, J. Appl. Phys. 24 (1953) 1232−1235.

[7] J.L. Bansal, Laminar flow through a uniform circular pipe with small suction, Proc. Natn. Acad. Sci. 32A (4) (1967) 368−378.

[8] R.M. Terril, An exact solution for flow in a porous pipe, ZAMP 33 (1982), 547-542.

[9] R.M. Terril, Laminar flow through a porous tube, ASME J. Fluids Eng. 105 (3) (1983) 303−306.

[10] S. Tsangaris, D. Kondaxakis, N.W. Vlachakis, Exact solution for flow in a porous pipe with unsteady wall suction/injection, Commun. Nonlinear Sci. Numer. Simul. 12 (2007) 1181−1189.

[11] B.J. Cox, J.M. Hill, Flow through a circular tube with permeable Navier slip boundary, Nanoscale Res. Lett. 6 (389) (2011) 1−9.

[12] J.V. RamanaMurthy, G. Nagaraju, P. Muthu, Micropolar fluid flow generated by a circular cylinder subject to longitudinal and torsional oscillations with suction/injection, Tamkang J. Math. 43 (3) (2012) 339−356.

[13] J. Srinivas, J.V. Ramana Murthy, Flow of two immiscible couple stress fluids between two permeable beds, J. Appl. Fluid Mech. 9 (1) (2016) 501−507.

[14] O.A. Bég, S.K. Ghosh, T.A. Bég, Applied Magnetofluid Dynamics, Modelling and Computation, Lambert, Germany, 2011, p. 445.

[15] R.M. Terril, G.M. Shrestha, Laminar flow through channels with porous walls andwith an applied transverse magnetic field, Appl. Sci. Res. 11 (1963) 134−144.

[16] H.A. Attia, Unsteady flow of a dusty conducting non-Newtonian fluid through a pipe, Can. J. Phys. 81 (2003) 789−795.

[17] Hazem A. Attia, Mohamed E.S. Ahmed, Circular pipe MHD flow of a dusty bingham fluid, Tamkang J. Sci. Eng. 8 (4) (2005) 257−265.

[18] Moustafa EL-Shahed, MHD of a fractional viscoelastic fluid in a circular tube, Mech. Res. Commun. 33 (2) (2006) 261−268.

[19] J.V. Ramana Murthy, N.K. Bahali, D. Srinivasacharya, Unsteady flow of a micropolar fluid through acircular pipe under a transverse magnetic field with suction/injection, Selguk J. Appl. Math. 11 (2) (2010) 13−25. http://journaldatabase.info/articles/unsteady_flow_micropolar_fluid_through.html.

https://doi.org/10.1016/j.heliyon.2019.e01281

[20] J.V. Ramana Murthy, K.S. Sai, N.K. Bahali, Steady flow of micropolar fluid in a rectangular channel under transverse magneticfield with suction, AIP Adv. 1 (2011), 032123.

[21] F. Mabood, S.M. Ibrahim, W.A. Khan, Framing the features of Brownian motion and thermophoresis on radiative nanofluid flow past a rotating stretching sheet with magnetohydrodynamics, Res. Phys. 6 (2016) 1015−1023.

[22] F. Mabood, S.M. Ibrahim, M.M. Rashidi, M.S. Shadloo, Giulio Lorenzini, Non-uniform heat source/sink and Soret effects on MHD non-Darcian convective flow past a stretching sheet in a micropolar fluid with radiation, Int. J. Heat Mass Transf. 93 (2016) 674−682.

[23] Shateyi Stanford, Fazle Mabood, Mhd mixed convection slip flow near a stagnation-point on a non-linearly vertical stretching sheet in the presence of viscous dissipation, Therm. Sci. 21 (6B) (2017) 2731−2745.

[24] G. Davaa, T. Shigechi, S. Momoki, Effect of viscous dissipation on fully-developed heat transfer of non-Newtonian fluids in plane laminar Poiseuille-Couetteflow, Int. J. Heat Mass Transf. 31 (2004) 663−672.

[25] B. Gebhart, Effects of viscous dissipation in natural convection, J. Fluid Mech. 14 (1962) 225−232.

[26] H.C. Brinkman, Heat effects in capillary flow I, Appl. Sci. Res. A2 (1951) 120−124.

[27] J.W. Ou, K.C. Cheng, Viscous dissipation effects on thermal entrance heat transfer in pipe flows with uniform wall heat flux, Appl. Sci. Res. 28 (1) (1973) 289−301.

[28] O. Anwar Bég, J. Zueco, H.S. Takhar, Unsteady magnetohydrodynamic Hartmann−Couette flow and heat transfer in a Darcian channel with Hall current, ionslip, viscous and Joule heating effects: network numerical solutions, Commun. Nonlinear Sci. Numer. Simul. 14 (4) (2009) 1082−1097.

[29] Nabil T. El Dabe, Galal M. Moatimid, Hoda S.M. Ali, Rivlin-Eriksen fluid in tube of variying cross section with Mass and Heat transfer, Z. Naturforsch. 57 (11) (2014) 863−873.

[30] Ahmet Z. Sahin, Rached Ben-Mansour, Entropy generation in laminar fluid flow through a circular pipe, Entropy 5 (5) (2003) 404−416.

[31] Rached Ben-Mansour, Ahmet Z. Sahin, Entropy generation in developing laminar fluid flow through a circular pipe with variable properties, Heat Mass Transf. 42 (1) (2005) 1−11.

https://doi.org/10.1016/j.heliyon.2019.e01281

[32] Nagaraju Gajjela, Anjanna Matta, K. Kaladhar, The effects of Soret and Dufour, chemical reaction, Hall and ion currents on magnetized micropolar flow through co-rotating cylinders, AIP Adv. 7 (115201) (2017) 1−16.

[33] Anjanna Matta, Nagaraju Gajjela, Order of chemical reaction and convective boundary condition effects on micropolar fluid flow over a stretching sheet, AIP Adv. 8 (115212) (2018) 1−11.

[34] S. Srinivas, A. Vijayalakshmi, A. Subramanyam Reddy, T.R. Ramamohan, MHD flow of a nanofluid in an expanding or contracting porous pipe with chemical reaction and heat source/sink, Propul. Power Res. 5 (2) (2016) 134−148.

[35] Odelu Ojjela, N.Naresh Kumar, Unsteady MHD mixed convection flow of chemically reacting micropolar fluid between porous parallel plates with soret and dufour effects, J. Eng. Math. (2016), 6531948, 13 pages.

[36] G. Nagaraju, J. Srinivas, J.V. Ramana Murthy, A.M. Rashad, Entropy generation analysis of the MHD flow of couple stress fluid between two concentric rotating cylinders with porous lining, Heat Transf. Asian Res. 46 (4) (2017) 316−330.

[37] G. Nagaraju, J. Srinivas, J.V. Ramana Murthy, O.A. Beg, A. Kadir, Second law analysis of flow in a circular pipe with uniform suction and magnetic field effects, ASME J. Heat Trans. 141 (1) (2018), 012004.

[38] S.J. Liao, Beyond Perturbation: Introduction to Homotopy Analysis Method, Chapman &Hall/CRC Press, Boca Raton, 2003. https://www.crcpress.com/Beyond-Perturbation-Introduction-to-the-Homotopy-Analysis-ethod/Liao/p/book/9781584884071.

[39] Fazle Mabood, W.A. Khan, Approximate analytic solutions for influence of heat transfer on MHD stagnation point flow in porous medium, Comput. Fluids 100 (2014) 72−78.

[40] F. Mabood, W.A. Khan, A.I.M. Ismail, Approximate analytical modeling of heat and mass transfer in hydromagnetic flow over a non-isothermal stretched surface with heat generation/absorption and transpiration, J. Taiwan Inst Chem Eng 54 (2015) 11−19.

[41] F. Mabood, W.A. Khan, Analytical study for unsteady nanofluid MHD Flow impinging on heated stretching sheet, J. Mol. Liq. 219 (2016) 216−223.

[42] F. Mabood, W.A. Khan, A.I.M. Ismail, Multiple slips effects on mhdcasson fluid flow in porous media with radiation and chemical reaction, Can. J. Phys. 94 (1) (2016) 26−34.

https://doi.org/10.1016/j.heliyon.2019.e01281

[43] S.M. Ibrahim, P.V. Kumar, G. Lorenzini, E. Lorenzini, F. Mabood, Numerical study of the onset of chemical reaction and heat source on dissipative mhd stagnation point flow of casson nanofluid over a nonlinear stretching sheet with velocity slip and convective boundary conditions, J. Eng. Thermophys. 26 (2) (2017) 256−271.

[44] Oluwole D. Makinde, Fazle Mabood, Mohammed S. Ibrahim, Chemically reacting on MHD boundary-layer flow of nanofluids over a non-linear stretching sheet with heat source/sink and thermal radiation, Therm. Sci. 22 (1B) (2018) 495−506.

[45] R.B. Bird, W.E. Stewart, E.N. Lightfoot, Transport Phenomena, John Wiley and Sons, New York, 1960. https://www.wiley.com/en-us/Transport+Phenomena%2C+Revised+2nd+Edition-p-9780470115398.

[46] A.B. Parsa, M.M. Rashidi, O. Anwar Bég, S.M. Sadri, Semi-computational simulation of magneto-hemodynamic flow in a semi-porous channel using optimal homotopy and differential transform methods, Comput. Biol. Med. 43 (9) (2013) 1142−1153.

[47] T. Hayat, T. Javed, M. Sajid, Analytic solution for MHD rotating flow of a second grade fluid over a shrinking surface, Phys. Lett. 372 (18) (2008) 3264−3273.

[48] R.A. Gardner, Laminar pipe flow in a transverse magnetic field with heat transfer, Int. J. Heat Mass Transf. 11 (6) (1968) 1076−1081.

[49] F.R. Cunha, Y.D. Sobral, Asymptotic solution for pressure-driven flows of magnetic fluids in pipes, J. Magn. Magn. Mater. 289 (2005) 314−317.

https://doi.org/10.1016/j.heliyon.2019.e01281